Ultimate Capacity of Corroded Statically Indeterminate Reinforced Concrete Members

Fernandez *et al. Int J Concr Struct Mater* (2018) 12:75
https://doi.org/10.1186/s40069-018-0297-9

International Journal of Concrete Structures and Materials

RESEARCH Open Access

Ultimate Capacity of Corroded Statically Indeterminate Reinforced Concrete Members

Ignasi Fernandez[1*], Manuel F. Herrador[2], Antonio R. Marí[3] and Jesús M. Bairán[3]

Abstract

The corrosion of steel reinforcement is commonly believed to be the primary cause of structural deterioration of reinforced concrete (RC) structures; as a result of this deterioration, a RC structure can incur a considerable reduction in structural serviceability and safety. Because of their inherent redundancy, statically indeterminate structures develop resistant mechanisms that can potentially assist in delaying the collapse of severely damaged RC structures. In order to experimentally demonstrate these resistant mechanisms, four groups of three two-span continuous RC beam members each were deteriorated using induced corrosion methods and tested to failure under monotonic loads. For control, one group of three RC beams was left uncorroded and similarly load tested. All the RC beam specimens subjected to corrosion demonstrated a significant reduction (a maximum reduction of 55% as compared to the uncorroded control group) of their ultimate capacity. The presence of corrosion induced a transition from flexural failure to anchorage failure in some specimens; despite the induced damage some redistributed structural capacity was observed. Modelling of deterioration effects by the inclusion of different aspects of corrosion was also conducted. Three-dimensional (3D) Finite-Element Method (FEM) models were developed to assess the variation in the mechanical properties of the corroded steel and the reduction in the bond interaction between concrete and steel due to the corrosion of the steel reinforcement. In general, the current 3D FEM models demonstrated a good agreement with the experimental data; however, 3D FEM models that exhibit greater sophistication are necessary to better describe the failure mode of some RC beam specimens when they are associated with local effects.

Keywords: statically indeterminate beams, reinforced concrete, corrosion, ultimate capacity, redistribution, bond, anchorage, 3D FEM modeling

1 Introduction

Structural safety is the most important requirement to be fulfilled in the design of reinforced concrete (RC) structures. A comprehensive understanding of the structural behaviour of RC structures is important for improving design quality and develop safe structure that can withstand varying loading combinations and environmental conditions. The corrosion of the steel reinforcement is commonly believed to be the most severe of the many factors that can result in the structural deterioration of RC structures. Several studies have concluded that the corrosion of steel reinforcement is the first natural cause of structural failure; these failures affect a large number of RC structures (Broomfield 2002). The structural performance of RC structures at service load levels is adversely impacted when corrosion leads to a reduction in the cross-sectional area and the potential reduction of the mechanical properties of the reinforcing steel (Apostolopoulos et al. 2016; Fernandez et al. 2015). The corrosion is hastened as a result of incremental increases in deflections and crack widths (along with the generation of new cracks) that create an environment for corrosion to advance. Moreover, the corrosion of reinforcing steel can directly impact structural safety by significantly reducing the carrying capacity (Ballim and Reid 2003; Cairns and Millard 1999; Val et al. 1998; Dang and François 2013; Tahershamsi et al. 2016) and/or the ductility of

*Correspondence: ignasi.fernandez@chalmers.se
[1] Department of Architecture and Civil Engineering, Division of Structural Engineering, Concrete Structures, Chalmers University of Technology, 412 96 Gothenburg, Sweden
Full list of author information is available at the end of the article
Journal information: ISSN 1976-0485 / eISSN 2234-1315

the RC structure thereby leading to the development of unexpected failure modes for which the RC structure has not been designed (e.g. brittle failures).

The corrosion of steel reinforcement structures has been widely studied by many researchers (Malumbela et al. 2009c; Cabrera 1996; Torres-Acosta et al. 2007; Rodriguez et al. 1997; Tahershamsi et al. 2014; Biondini and Vergani 2014; Coronelli 2002). Researchers have conducted experiments to determine the impacts of corrosion; however, these experiments have primarily focused on basic structures (such as simply supported beams), where the global response is directly related to the response of the critical section. Some researchers have been forced to work with reduced test setups as the development of experimentation in the field of corrosion has been hindered by the complexity of the corrosion phenomena and by the complicated experimental setup required to perform accelerated corrosion testing.

The observations and findings presented herein correspond to the second and last phase of the analysis completed within a study on the structural effects of steel reinforcement corrosion on statically indeterminate RC members; the referenced study utilised two-span continuous RC beams subject to the effects of corrosion as the basis for testing (Fernandez et al. 2016c). The steel reinforcement within twelve statically indeterminate RC beams (divided into four groups of three) was subjected to varying levels of impressed current; these RC beams were subsequently loaded to failure. This paper presents the effects of steel reinforcement corrosion on the carrying capacities of the RC beams. The current density applied to the reinforcement was defined using second Faraday's Law theory (El Maaddawy and Soudki 2003; Caré et al. 2008; Lu et al. 2011; Austin et al. 2004). For control, one group of three RC beams was left uncorroded. No steel reinforcement stirrups were utilised within the RC beams in order to avoid an electrical connection from occurring between the top and bottom longitudinal steel reinforcement bars; as a consequence, premature push-out of the outermost longitudinal reinforcement bars took place near the supports at loading (Fig. 1c). Because of the premature reinforcement push-out three RC beams without strengthening were tested to failure. The remaining RC beams were strengthened by laterally confining the ends of the beams, which significantly increased the bond capacity between the steel reinforcement and the concrete. During the incremental loading-to-failure process structural and corrosion parameters of the RC beams were monitored and evaluated.

The final stage of the study consisted of performing numerical analyses of the RC beam specimens utilising a three-dimensional (3D) Finite-Element Method (FEM) model ('DIANA' by TNO Diana BV); the results from the numerical analyses were then compared to the results of the RC beam tests. The impact of the local corrosion phenomena was observed to result in a reduction of the steel reinforcement bar cross-sectional area (with a corresponding reduction in the bar perimeter) and the degradation of the bar's mechanical properties. The bond-slip relationship was implemented by utilising an embedded reinforcing steel approach with interface elements including a non-linear bond relationship to the concrete. The scope, suitability, and advantages and disadvantages of the completed modelling have been previously studied (Tahershamsi et al. 2017).

2 Experimental Programme

The present work is a part of a larger experimental study that utilised twelve statically indeterminate beams simulating strips of slabs subjected to accelerated corrosion.

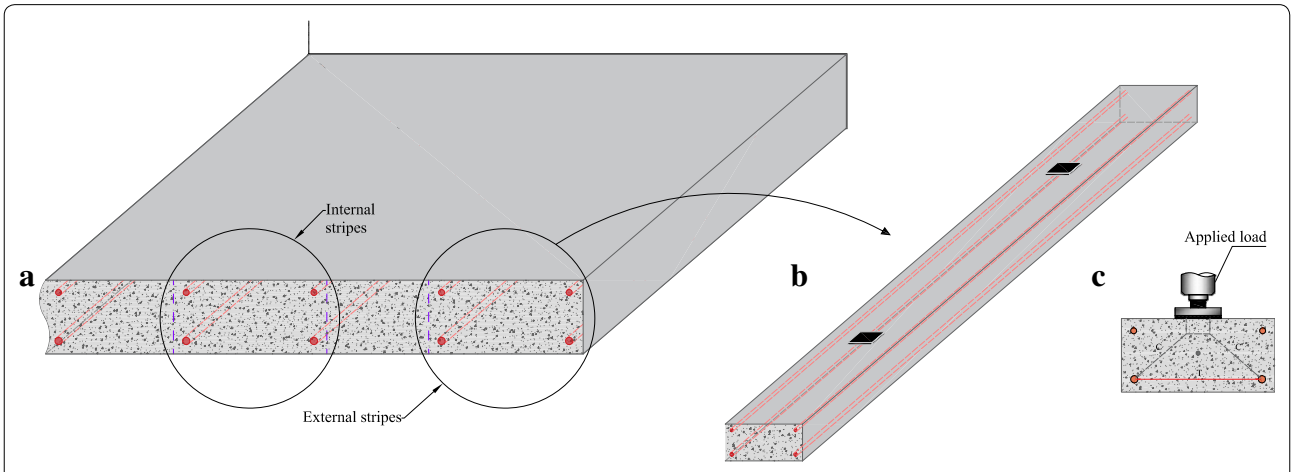

Fig. 1 **a** Slab representing internal and external stripes. **b** Beam description. **c** Strut-and-tie mechanism developed in the cross-section at loading.

Table 1 Concrete properties.

	Specimen	Compressive strength (MPa)	Average	Tensile splitting strength (MPa)	Average	Modulus of elasticity (MPa)	Average
Group 1	*G1_2P*	43.03	41.79	3.38	3.35	37,816	36,798
	G1_P	41.40		3.67		37,241	
	G1_SW	40.93		3.00		35,336	
Group 2	*G2_2P*	39.36	39.09	2.70	2.65	36,165	35,615
	G2_SW	36.81		2.57		33,929	
	G2_P	41,10		2,69		36,752	
Group 3	*G3_SW*	37.64	38.43	2.70	2.60	37,605	36,598
	G3_P	38.55		2.62		35,204	
	G3_2P	39.11		2.49		36,984	
Group uncorroded	*GR_2P*	38.61	38.36	2.64	2.83	36,795	37,097
	GR_P	38.28		2.67		36,825	
	GR_SW	38.20		3.17		37,670	

The first part of this study was centred on the evaluation of specimen serviceability during the corrosion development phase (Fernandez et al. 2016c); the work presented within this paper focuses on the ultimate state behaviour of identical test pieces. The RC beam specimens, which had been subjected to constant service loads until the desired degree of corrosion was attained, were unloaded, and then progressively loaded again to failure. The ultimate capacity of the concrete specimens was assessed by measuring several physical parameters (e.g. deflections, reactions, strains in concrete and steel, crack widths, etc.).

2.1 Material Properties

Concrete compressive strengths and the moduli of elasticity were determined at 28 days after casting utilising a compression-testing machine. Three cylindrical 150×300 mm specimens were tested for each type of concrete. The splitting tensile strength of concrete was obtained by means of the Brazilian Test. Table 1 details the mechanical properties and moduli of elasticity of all of the concrete specimens (tested following 28 days of curing). Specimen nomenclature as utilised within Table 1 is as follows:

- GR, G1, G2, and G3 indicate different corrosion levels, from "reference" (uncorroded) to the most corroded, according to the accelerated corrosion setup shown in Sect. 2.3.
- SW, P, 2P indicate different dead load levels applied during the corrosion process; respectively, self-weight, load just below service design values and twice that load (over service design value).

Table 2 Steel properties.

Diameter (mm)	Yielding stress (MPa)	Ultimate stress (MPa)	e_y (—)	e_u (—)	Modulus of elasticity (MPa)
10	550	650	0.0025	0.11	200,000
12	545	643	0.0027	0.12	195,000

The tensile strength of the steel reinforcement bars (400 mm-long) utilised within the RC beam tests was determined using a tensile testing machine. The modulus of elasticity in the elastic range was ascertained and the complete stress–strain curve was recorded by utilising three displacement transducers to obtain the longitudinal strains of the steel reinforcement under the applied load up to the point of load failure. Table 2 shows the different material properties of the 10 and 12 mm diameter (ø) deformed steel reinforcement bars.

2.2 Description of Specimens

Twelve continuous two-span RC beams were cast. The RC beam specimens were 5000 mm in overall length with two symmetric spans of 2400 mm between the support axes. The rectangular cross-section of the RC beam was 250 mm in width and 120 mm in depth. Concrete cover was 15 mm on all four beam faces. Longitudinal steel reinforcement within the RC beam was arranged in order to avoid a potential direct electrical connection between the top and the bottom steel reinforcement bars; this preventative placement measure was aimed to prevent interference in the corrosion process. The intentional absence of steel reinforcement stirrups and the RC beam's cross-sectional shape closely represents the characteristics of corroded RC slabs (Fig. 1a). Beams representing two different zones of a corroded slab were tested: first zone,

edge parts of the slab (where it might be possible to identify areas without stirrups and hence no lateral confinement); and, second zone, internal zones of the slabs (the most common situation where the entire specimen is confined by the surrounding concrete).

Three out of twelve RC beams were unstrengthened; this unstrengthened situation represented the edge of the slab or 'external strips'. Conversely, to simulate 'internal strips', the remaining RC beam specimens were fitted with external passive strengthening to provide confined conditions, as illustrated in Fig. 1a. The push-out effect due to the inclination of the struts in the transverse direction within the RC beam specimens was avoided with the addition of the passive strengthening and therefore a more realistic behaviour of the studied structural member could be reproduced in the laboratory.

The internal mechanistic scheme of truss and ties that was responsible for the push-out effect depicted in Fig. 1b. As illustrated within Fig. 1b, a truss was formed to transfer the applied load from the hydraulic jack to the tensile longitudinal steel bars; this truss can be figuratively decomposed into forces P1 and P2. Available concrete between the tensile bars and the hydraulic jack could withstand vertical force component P2. Conversely, the horizontal force component P1 (which in normal condition would be sustained by the adjacent slab section) is pushing out the steel reinforcement bar resulting of insufficient concrete resisting the push-out force. Observations indicate that the absence of stirrups can lead to a detachment of the reinforcing steel from the RC beam concrete section. Figure 2a depicts the overall view of the RC beam whereas Fig. 2b describes the detailed geometry of the RC beam cross-section and the steel reinforcement layout at critical points. A description of the passive strengthening configuration can be seen in Fig. 2c.

2.3 Accelerated Corrosion

The corrosion of the steel reinforcement was forced using an impressed current. Following Faraday's Law (Eq. 1), it is possible to estimate the weight loss of steel due to corrosion, knowing the applied intensity over time, I(t),

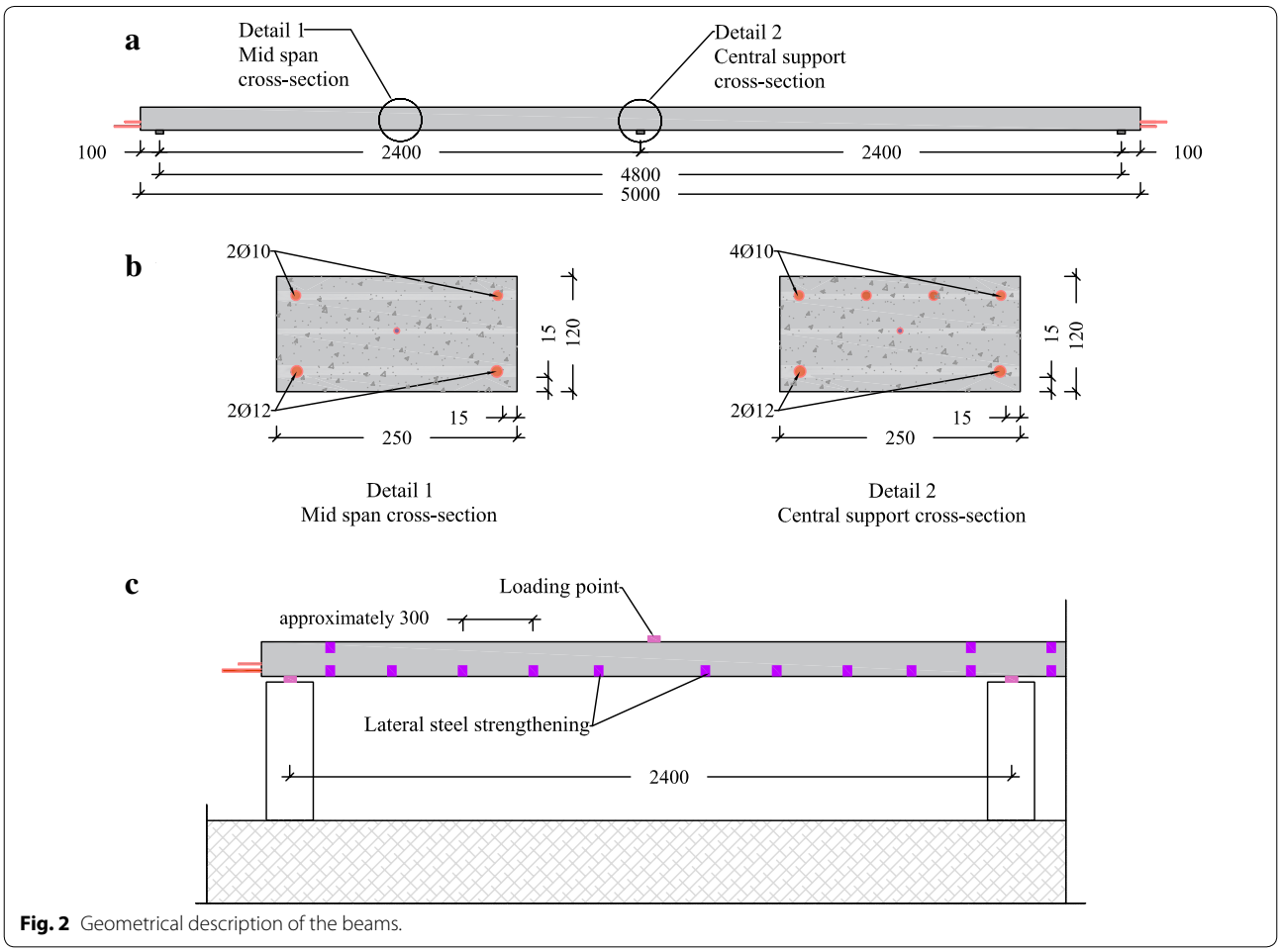

Fig. 2 Geometrical description of the beams.

and the geometrical bar properties such as diameter and exposed bar length.

$$E = \frac{m_{Fe} \cdot \int I \cdot dt}{V \cdot F} \quad (1)$$

In Eq. (1): m_{Fe} is the atomic mass, V is the steel valence (taken as equal to two) and F is Faraday's constant.

As the applied intensity was constant during the test, it is possible to rewrite Faraday's Law as Eq. (2).

$$\Delta m = \frac{m_{Fe} \cdot I \cdot t}{V \cdot F} \quad (2)$$

In this study, current densities below 350 μA/cm^2 were applied in order to corrode the steel reinforcement bar specimens; by taking this current density value into account, it was possible to estimate the different exposure times for each specimen according to the target corrosion level. Each group of RC beams, numbered G1, G2, and G3 (Group GR being the uncorroded reference group), was exposed to an impressed current for a period of 42, 56 and 100 days, respectively. Accordingly, the estimated corrosion level for each group was 10% (56 days), 15% (42 days) and 20% (100 days).

RC beams to be corroded were placed over two pools situated under each of the free span areas. A 6 mm diameter stainless steel wire situated in the centre of the RC beam cross-section was routed along the beam length to act as the cathode and the steel reinforcement (or 'rebar') was to act as the anode within the corrosion circuit. An irrigation system consisting of a porous tube discharging water on the top face of the RC beam kept the beam wet throughout the exposure time. Concrete moisture had to be maintained at a high level in order to facilitate the corrosion process; adding 4% in cement weight of sodium chloride (NaCl) to the water mixture during casting further served to reduce the resistivity of the concrete as the NaCl served as an electrolyte within the corrosion cell. It was possible to connect different RC beam specimens in series; this wiring ensured that the impressed current would be identical for every specimen in the circuit (Fig. 3). In the presented work, corrosion rates below 350 μA/cm^2 were applied in order to corrode the specimens. Further details of the corrosion setup are provided within reference (Fernandez et al. 2016c).

2.4 Measurement Equipment

Several measurement instrumentation systems were placed on each of the RC beams in order to measure and assess the physical changes incurred during both of the following study phases: the corrosion under constant load phase; and, the loading to failure phase. Load cells were placed at the two external supports and at the two mid-spans (corresponding to where the point loads were applied) thereby allowing the reaction at the central support to be obtained by equilibrium. All load cells complied with Organization Internationale

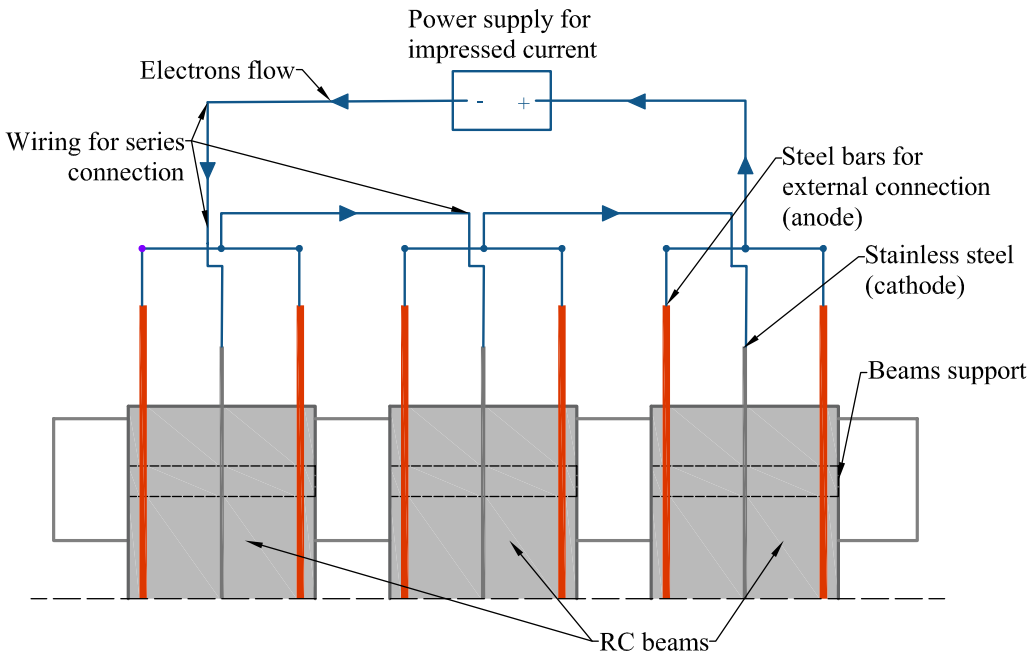

Fig. 3 Connection setup for accelerated corrision.

de Metrologie Legale (OIML) Standard R60. OIML R60 Class C load cells (1000 divisions) measured the loadings to a resolution of 0.5 kg and exhibited a total error of less than ± 0.05%. The RC beams were tested to failure in the same location where corrosion under constant load took place and the same load cells were utilised to calculate the bending moment. Strain gauges were placed at selected points along both the compressive and tensile steel reinforcement bars. Ten strain gauges were placed on each RC beam to measure the tensile and compressive strains at both mid-span cross-section and at the central support cross-section during the corrosion and the loading to failure phases. The strain gauges attached to the steel reinforcement bars were protected from physical and corrosive damage by means of encapsulation. During the corrosion phase the encapsulation of the strain gauges served to mitigate the potential for water, rust and/or cement intrusion from interfering with the strain gauges. In some instances, water and/or rust managed to penetrate the protective encapsulation, which resulted in a non-functioning strain gauge; failure of the strain gauges due to a breach of the encapsulation occurred at a greater frequency within the highly corroded RC beam specimens. Most of strain gauges utilised on the uncorroded RC beam specimens functioned satisfactorily throughout the testing to failure phase. In addition to the strain gauges, linear variable differential transformers (LVDTs) were placed at the two mid-span positions to measure deflections during both the corrosion and loading-to-failure phases. The detailed positioning of the different sensors is illustrated in Fig. 4.

2.5 Loading Test Setup

Two load frames anchored to the laboratory testing slab and two identical hydraulic jacks (connected in parallel to the same pressure supply) were utilised in order to introduce two equal loads to the mid-spans of each tested beam. The loads exerted by the hydraulic jacks were systematically applied by means of displacement control; two load cells recorded the applied forces to the point of beam failure. Neoprene bearing pads (20 mm thickness) were placed under the two applied load points and under the two external points of support. Figure 5 illustrates the loading test setup.

2.6 Pull-Out Tests

Eight direct pull-out tests were performed on separate concrete specimens to characterise the strength of the bond between the same types of reinforcement steel and concrete. The recognised assertion for short pull-out tests (utilising ribbed (i.e. deformed) steel reinforcement bars, defined by an embedment length of less than five times the bar diameter) is that the distribution of bond stresses is uniform along the bonded portion (Losberg 1962; Ruiz et al. 2007). Accordingly, the uniform bond stress hypothesis was utilised; as a result, the local bond stress could be estimated by the formula in Eq. 3.

$$\tau = P/\pi \Phi L \tag{3}$$

In Eq. (3): P is the applied load (N), Φ is the nominal diameter of the steel bar (mm), and L is the embedded length (mm).

The experimental setup for the pull-out testing complied with *UNE-EN 10080:2006* code recommendations (UNE-EN_10080 2006). Steel bars of ϕ12 mm were embedded into the centre of eight 200 mm cubic concrete specimens. The steel bars completely traversed the 200 mm cube section. A segment of plastic tube was utilised to debond 140 mm of the steel reinforcement bar from the concrete, leaving the remaining 60 mm length of bar to bond with the surrounding concrete (Fig. 6). The passive slip between concrete and steel reinforcing was measured during the pull-out test. An LVDT was affixed to the bottom of the concrete cube in order to register the total slip of the reinforcing steel. A hydraulic jack clamp was affixed to the end of the steel reinforcement bar. A load was then applied directly to the steel reinforcement bar at a constant rate of 0.2 mm/min (by means of control displacement) to the point of failure in order to describe the pre- and post-peak bond behaviour and the residual bond capacity. The applied load and the LVDT readings were recorded every half a second by means of a data acquisition system. Details of the experimental pull-out test setup are illustrated at Fig. 6.

3 Experimental Results

Table 3 details the ultimate load achieved on each RC beam and the degree of corrosion attained (quantified as the uniform percentage of steel loss) at the end of the corrosion phase. RC beam specimen G3_2P failed under the service load applied during the corrosion phase; the significant reduction in the ability of G3_2P to accommodate the applied load was a marked departure from the loading capacities exhibited by the other RC beam specimens. The corrosion of the steel reinforcement within G3_2P was very severe resulting in a steel loss of up to 24%. In addition, intense localised corrosion of the G3_2P tensile steel reinforcement was observed in the central support cross-section following the cleaning process by sandblasting of the bars for the rust removal (Fernandez et al. 2018). Several corrosion pits were observed in two segments of the G3_2P tensile reinforcing steel; the advanced state of corrosion effectively cut completely through the reinforcing steel leading to the structural collapse of the RC beam. The deflections that were recorded

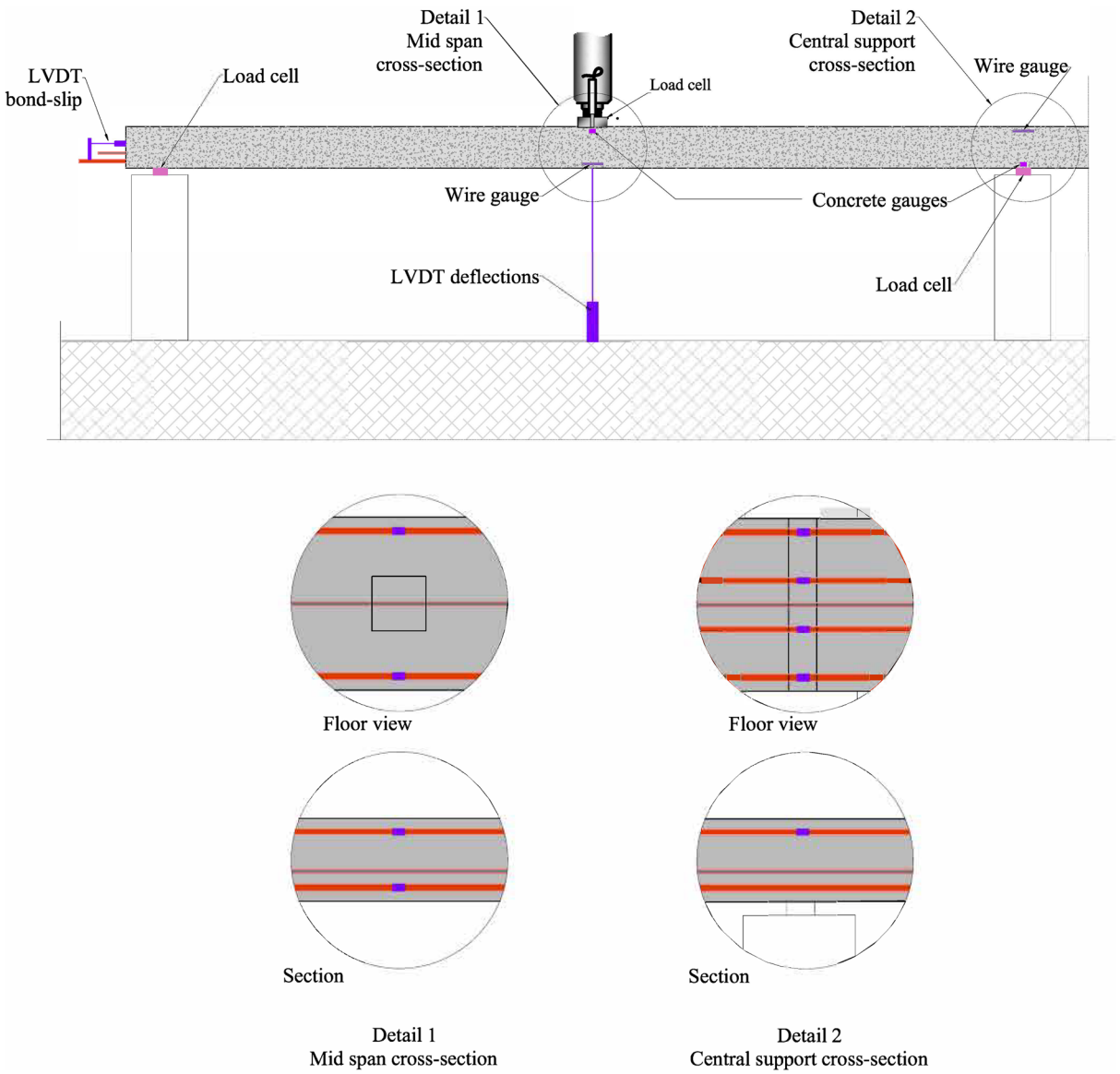

Fig. 4 Arrangement of the external measurement equipment; strain gauges for concrete, L VDT's and load cells. Arrangement of strain gauges for steel reinforcement.

just prior to the failure of the G3_2P beam were not particularly significant so the structural failure was considered to be completely a result of brittle failure.

3.1 Description of Specimen Damage Prior to Load Testing

The corroded RC beams were observed to be highly deteriorated due to the induced steel corrosion. Longitudinal cracks aligning approximately with the top and bottom reinforcement of all RC beam specimens were observed; this longitudinal cracking was attributed to rust expansion. RC beams loaded during the induced corrosion procedure exhibited three transverse cracks: a transverse crack appeared at each mid-span location (under the applied load point); and, the third transverse crack appeared over the central support (within the negative bending moment zone). The by-products of the corrosion process were highly visible in the form of rust stains along the RC beam member (Fig. 7).

3.2 Results of the Structural Behaviour of Tested Specimens

3.2.1 Uncorroded RC Beam Members

Uncorroded beams exhibited a ductile flexural failure mechanism. Both the top and bottom steel reinforcement

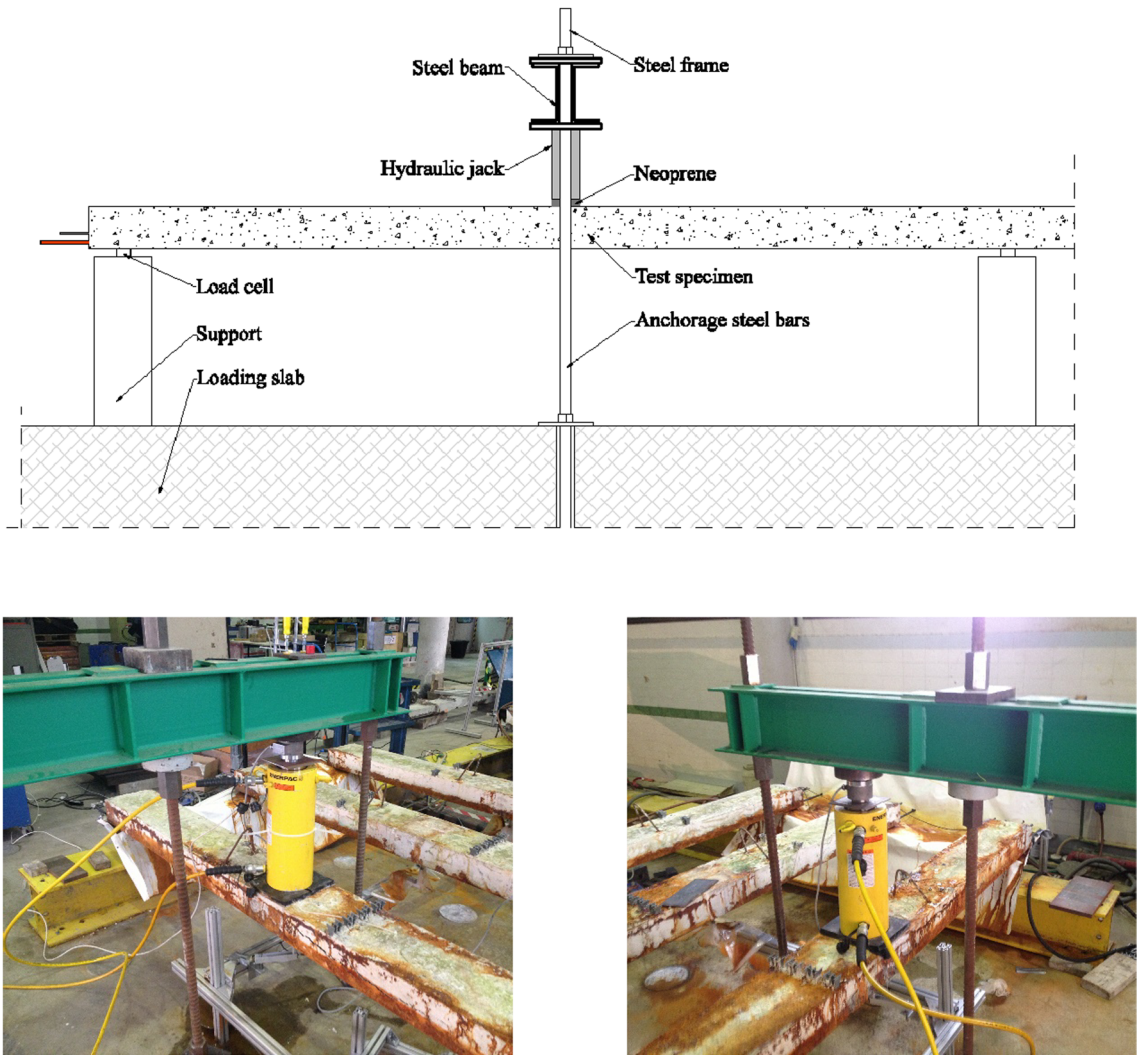

Fig. 5 Test configuration during load to failure.

yielded demonstrating high ductility at failure. The ultimate applied load was around 36 kN. The load–displacement curves for the three uncorroded members are illustrated within Fig. 8. Up to a 10% redistribution of moments between the weaker and the stronger structural sections was observed (Fig. 9). Given the nature of the uncorroded RC beam specimens this re-distribution of moments behaviour was anticipated. Figure 10 illustrates the steel reinforcement strains (as measured by strain gauges) within the GR_P beam sections directly under the point of applied loading and directly above the central support; both critical cross-sections yielded in bending.

3.2.2 Corroded RC Beam Members

Figure 11 illustrates the overall load deflection for the corroded internal slab strips (laterally strengthened beams) compared to deflections associated with the uncorroded RC beam members. Corroded RC beams were observed to have comparative structural responses amongst themselves by exhibiting similar load capacities regardless of the respective levels of reinforcing steel corrosion. The loadings at RC beam failure ranged between 20 and 25 kN; these failure loadings represent of a load reduction ranging between 30 and 46% as compared to the failure loadings of the uncorroded RC beam specimens. Despite the reduction in bearing capacities, the observation of large deformations prior to failure of the corroded RC beams indicated that ductility was present at the time immediately preceding beam failure. The corroded RC beam specimens exhibited similar displacements at ultimate load as the uncorroded RC beam references.

Redistribution of internal forces within corroded RC beam specimens was observed in some specimens as

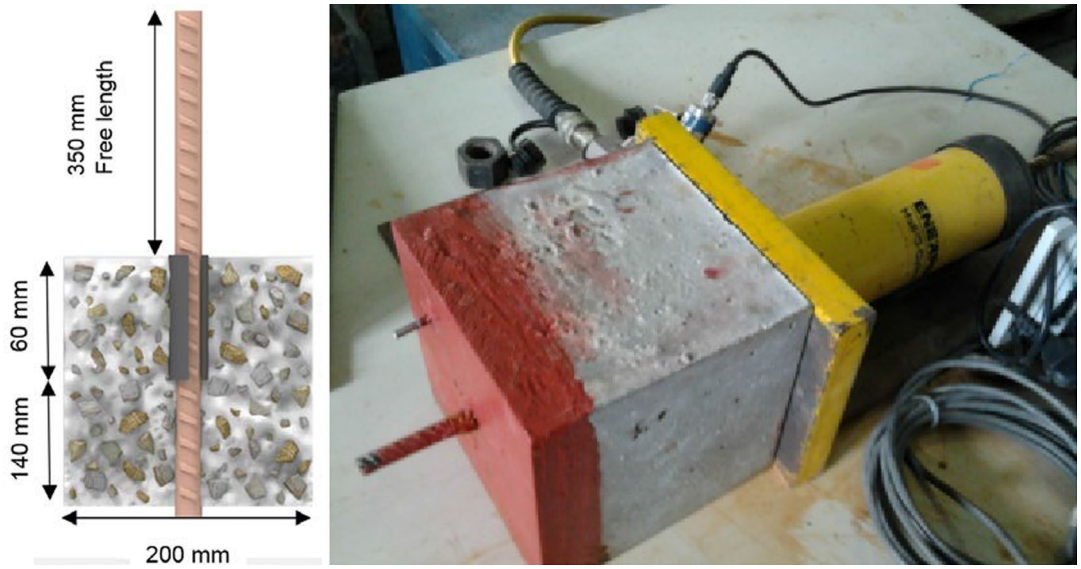

Fig. 6 Pull-out specimen description and test setup.

Table 3 Measured corrosion levels, exposure days, permanent load during corrosion and ultimate applied load on span centre at failure.

	Specimen	Exposure time (days)	Steel loss (% top/bottom reinforcement)	Permanent load (kN)	Ultimate load (kN)	Loss of capacity (%)
Group 1[a]	*G1_2P*	56	6/14	16.50	24.50	29
	G1_P		6/12	6.74	24.75	29
	G1_SW		9/11	0.00	11.40	67
Group 2	*G2_2P*	42	6/15	17.70	25.75	26
	G2_SW		6/10	0.00	21.00	39
	G2_P		7/15	8.34	24.75	29
Group 3	*G3_SW*	100	15/15	0.00	21.80	37
	G3_P		17/20	8.47	21.00	39
	G3_2P		10/24	17.50	17.50[b]	56
Group Uncorroded	*GR_2P*	–	–/–		31.60	–
	GR_P				36.59	–
	GR_SW				36.42	–

[a] Beams without lateral strengthening.

[b] Beam failed under permanent load.

depicted in Fig. 12. The consequences of corrosion (i.e. steel cross-section reduction, degradation of reinforcing steel mechanical properties, concrete splitting cracks) are readily apparent when one compares the observations presented within Fig. 12 (corroded RC beams) to those observations within Fig. 9 (uncorroded RC beams). Within corroded RC beam members, the difference between the moment at the central support and the mid-span moment was more pronounced than those respective moments observed in the uncorroded RC beam specimens. The difference in moments indicates that the structural capacity and the stiffness of the corroded specimens were markedly reduced because of the deterioration of reinforcing steel due to corrosion.

Corroded RC beam specimens G2_P and G3_SW exhibited critical end slips at the bottom reinforcement (Fig. 13). The advanced extent of reinforcing steel deterioration due to corrosion led to a significant drop in anchorage capacity; the loss of anchorage capacity led to the reduction in the load capacity of the corroded RC

Fig. 7 Deterioration at the end of the accelerated corrosion process: (left) longitudinal and (right) transverse cracks.

beam member. Reinforcement slip occurred within corroded RC beam specimen G3_SW at very low levels of loading. The observation of the G3_SW reinforcement slip indicates that a reduced bond between the reinforcing steel and the concrete was the result of corrosion that in turn led to the decreased effectiveness of the provided lateral confinement. Conversely, corroded RC beam specimen G2_P displayed a brittle bond failure. There was minimal reinforcement slip at very low load levels; however, when the applied load reached 25 kN the bond between the concrete and steel drastically diminished triggering severe reinforcement slippage that subsequently led to the reduced load capacity of the corroded RC beam.

Figure 14 illustrates the overall structural behaviour of the corroded external RC beam strips (unstrengthened beams) as compared to the structural behaviour of the uncorroded RC beams. All the external strip members exhibited anchorage failures. Figure 15 details the final state of the unconfined RC beams (G1_2P, G1_P, G1_SW). Concrete splitting and concrete cover spalling was observed and the damage attributed to the push-out effect; the push-out mode of failure was not prevented by the presence of external confinement. The level of reinforcing steel corrosion that the external strip group realised was sufficient to alter the failure mode from bending to anchorage failure (even though this external strip group experienced the least corrosive effects). Figure 16 illustrates the evolution of the strain (strain gauge readings) within the bottom steel reinforcement with respect to the measured deflection of the RC beam; for the purposes of comparison a second vertical axis representing the evolution of the loading is also presented within Fig. 16. Reinforcement slip occurred within the bottom reinforcement steel following the application of a 10 kN load; the reinforcement slip led to the aforementioned anchorage failure. A constant stress value within the reinforcing steel was a result of the remaining bond capacity. The loading capacities of the external strip members were reduced up to 55% as compared to the loading capacities of the uncorroded specimens. As foreseen, the significant reduction in load redistribution and redundancy was the result of the failure being premature and more brittle.

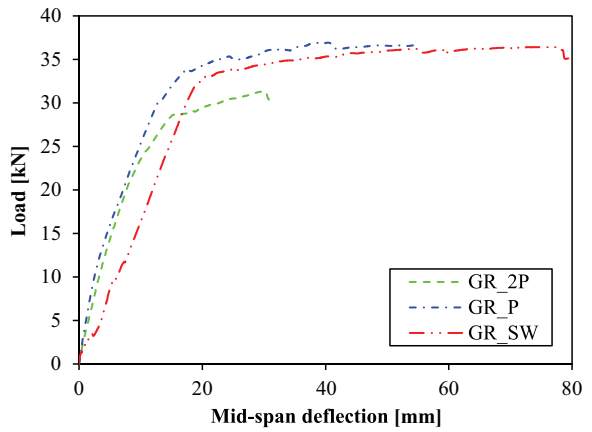

Fig. 8 Load vs. mid-span deflection curves for uncorroded specimens.

Figure 17 details the anchorage failure of RC beam specimen G1_P; measured end-slip is compared to both the strains recorded within the bottom reinforcing steel bar (Fig. 17a) and to the applied load (Fig. 17b). The reduction of stress on the bottom reinforcement as reinforcement slip increases (until residual bond capacity is reached) is illustrated within Fig. 17a. Figure 17b also illustrates the anchorage failure mode; from this figure, we can see that the remaining bond capacity allowed the recovery of some load capacity after anchorage failure occurred.

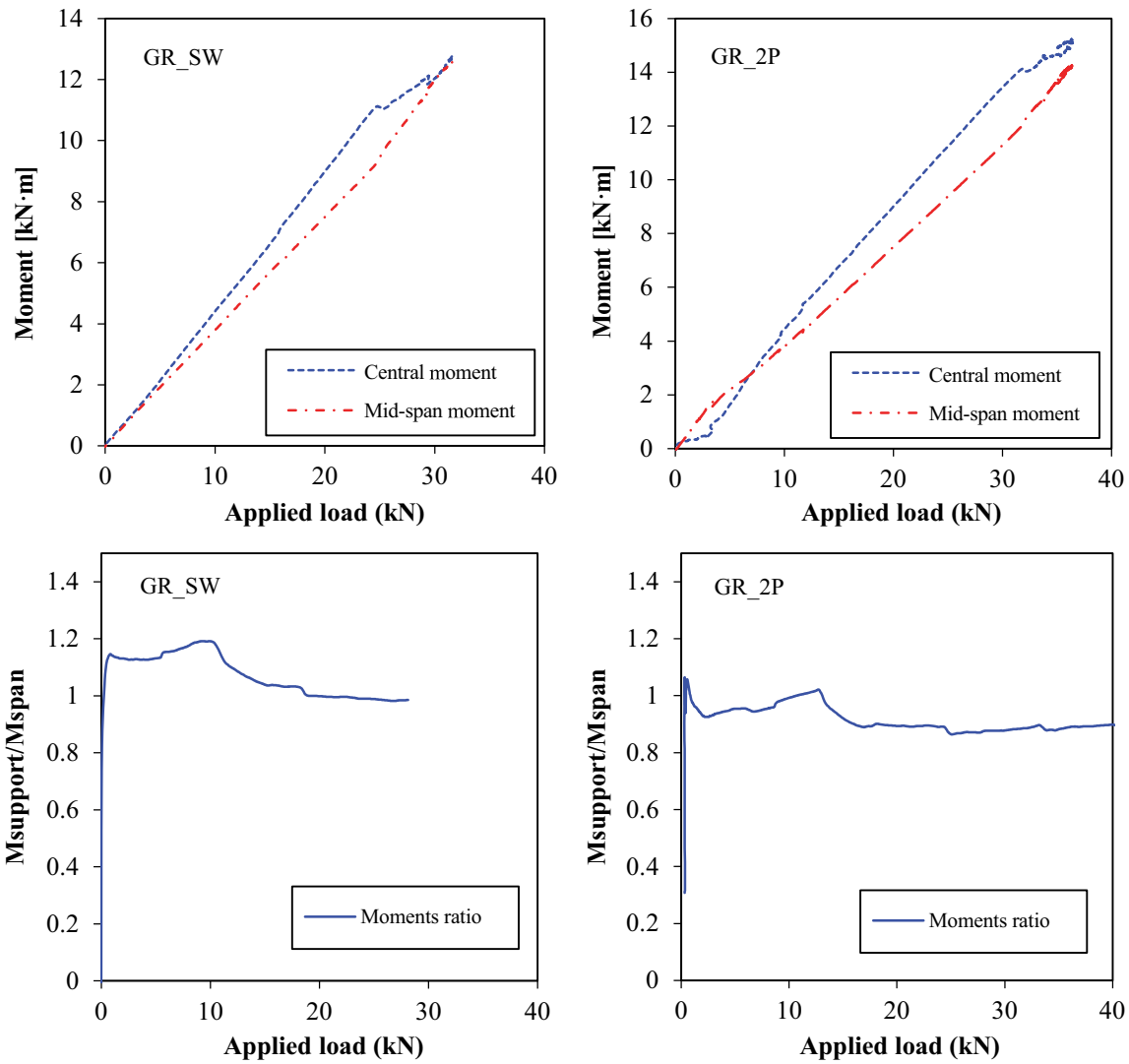

Fig. 9 Bending moment vs. applied load (top) and internal forces redistribution for uncorroded.

3.3 Discussion of the Experimental Results

Experimental observations support that the ultimate capacity of the tested, statically indeterminate RC beam members was clearly reduced when corrosion of the steel reinforcement occurred.

Brittle and premature failures of the corroded external strips (unstrengthened RC beams) due to anchorage failures was noted. The lack of transverse steel in conjunction with the impacts of the corroded reinforcing steel contributed to local splitting failures and the subsequent decrease in bond capacity of the bottom reinforcement. The remaining bond capacity between the reinforcing steel and the concrete was not sufficient to transfer the applied forces; and, as a result, the load capacity of the corroded external strip RC beams was significantly reduced (even though the corrosion level within these external strips was not as pronounced as other members).

The internal RC beam strips (laterally strengthened beams) provided superior overall structural characteristics as compared to the structural characteristics of the external RC beam strips. Despite being exposed to higher corrosion levels, the internal RC beam strips exhibited a higher total load capacity than that of the external strips; the increase in load capacity was attributed to the confinement provided by external passive strengthening that ensured preservation of some bond capacity and avoided premature failure due to push-out effects. All of the internal RC beam strips failed when subjected to the same approximate failure loadings; failure was independent of the respective corrosion levels. The independence

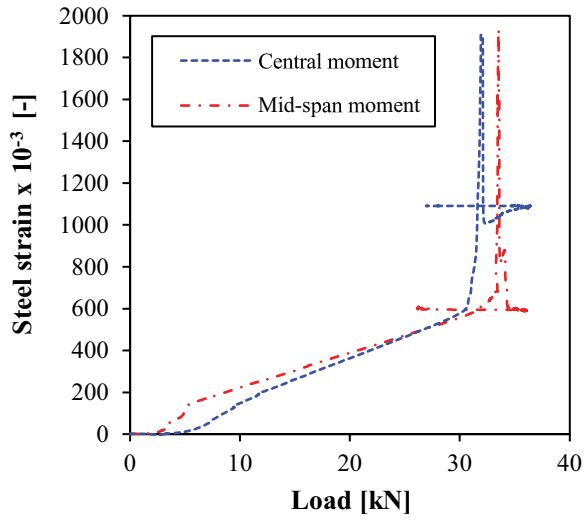

Fig. 10 Steel strain reinforcement vs. load, at mid-span and over central support in beam GR_P.

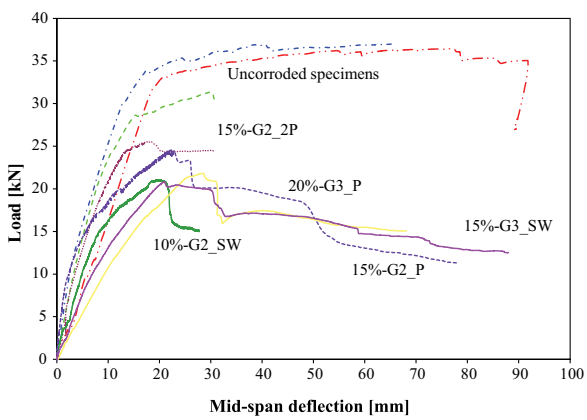

Fig. 11 Load vs. mid-span deflection curves for corroded, laterally strengthened beams and uncorroded beams.

between the approximate singular failure loading and the varied corrosion levels of the internal RC beam strips may initially appear counter-intuitive; however, the explanation of this behaviour can be explained by the redistribution capacity (inherent to redundancy) of the statically indeterminate RC elements., The loss of steel in highly damaged cross-sections produces increased displacements, which in turn generate secondary (compatibility) moments in a statically indeterminate structure (based upon the assumption that no loss of anchorage is produced by corrosion before flexural failure occurs). These secondary moments reduce moment demand in the highly damaged zone while increasing the moment in the less damaged regions. Global equilibrium can be attained without collapse of the structure if these damaged sections exhibit sufficient flexural capacity to withstand the increased moment demand. In summary, the structural redundancy generates a beneficial indirect effect (reduction of the demand in deteriorated cross-sections) in opposition to the directly harmful effect produced by corrosion of the reinforcing steel (i.e. reduction of cross-section capacity) thereby mitigating a reduction in carrying capacity.

The redistribution/redundancy effect was clearly exhibited by RC beam specimen G3_2P when the structure failed under dead weight load conditions because of extreme corrosion of the reinforcing steel (i.e. local corrosion severed one of the tensile reinforcing steel bars at the mid-span). High strains at the mid-span cross-section triggered a moment redistribution towards the less damaged part of the structure (i.e. central-support section). The maximum capacity of the G3_2P cross-section (with consideration that only one tensile bar was present) was attained at approximately $t=71$ days (Fig. 18). From $t=71$ days, to failure of the structure occurring at approximately $t=100$ days, the moment at the G3_2P damaged section was progressively reduced. The reduction in moment made it possible for the damaged section to sustain the applied load in spite of the increased damage; therefore, the redistribution capacity of the continuous beam prevented premature failure of the structure.

Because all the RC beam specimens exhibited a change in the failure mode towards bond-induced failure it is our contention that the redistribution mechanism was sufficiently enabled to guarantee the global stability of the beams until bond capacity was exhausted. Adverse effects of a highly corrosive environment (i.e. reduction of steel cross-section, degradation of steel mechanical properties) did not influence the structural behaviour of the RC beams as much as the bond capacity (very strong confinement conditions would be needed to avoid anchorage failure in these conditions). The effects of reinforcing steel corrosion (i.e. concrete cover spalling, concrete mechanical properties degradation, steel cross-section reduction, steel mechanical properties degradation) may have a greater influence on structural performance at low corrosion levels where the bond between the concrete and the steel has not markedly deteriorated.

3.4 Pull-Out Test Results

The results of the pull-out tests utilising ø12 mm reinforcing steel are detailed within Fig. 19. The average τ_{max} observed was τ equals 1.74 MPa. Figure 19 also provides a comparison with the local bond-slip curves presented within the CEB-FIP Model Code 90 (fib Model Code 1990). The bond-slip curves presented within CEB-FIP Model Code 90 overestimate the observed experimental

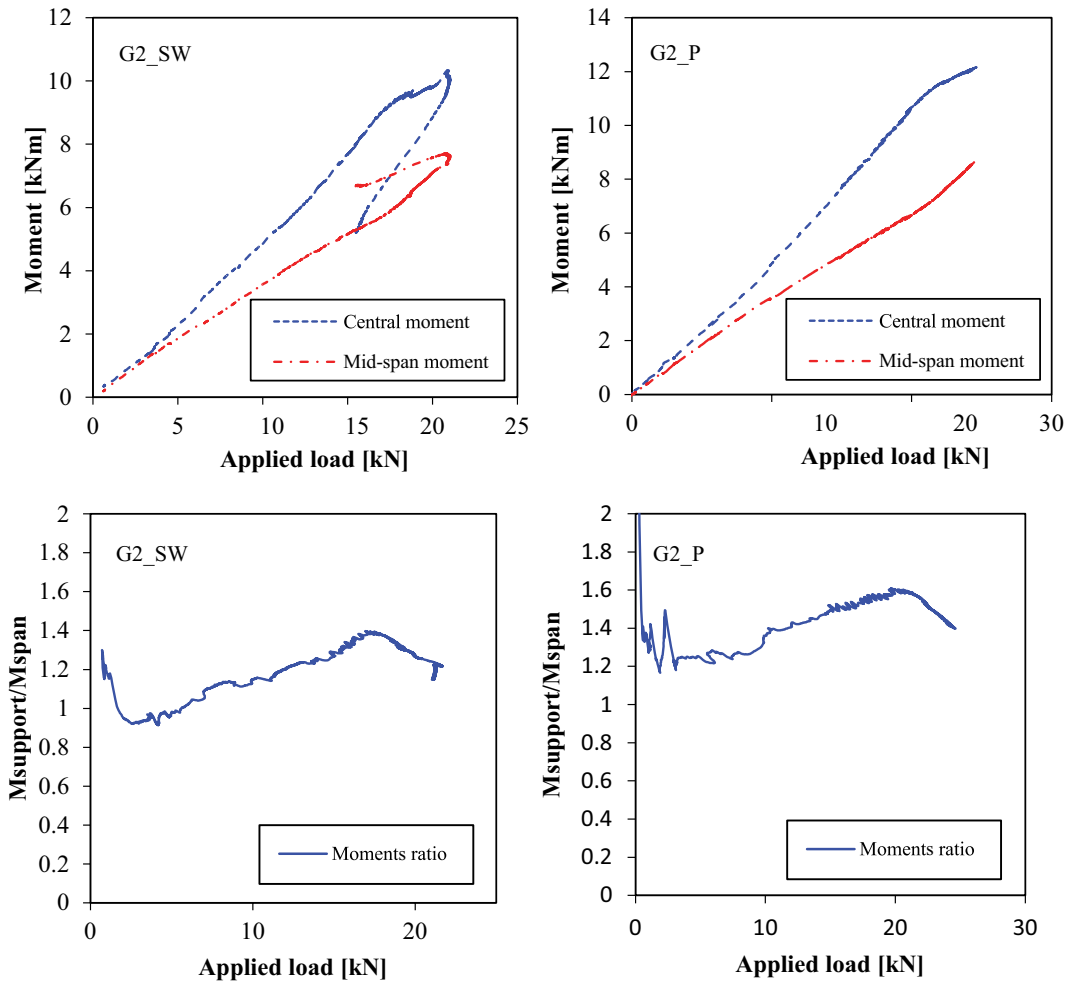

Fig. 12 Bending moment vs. applied load for corroded, laterally strengthened beams.

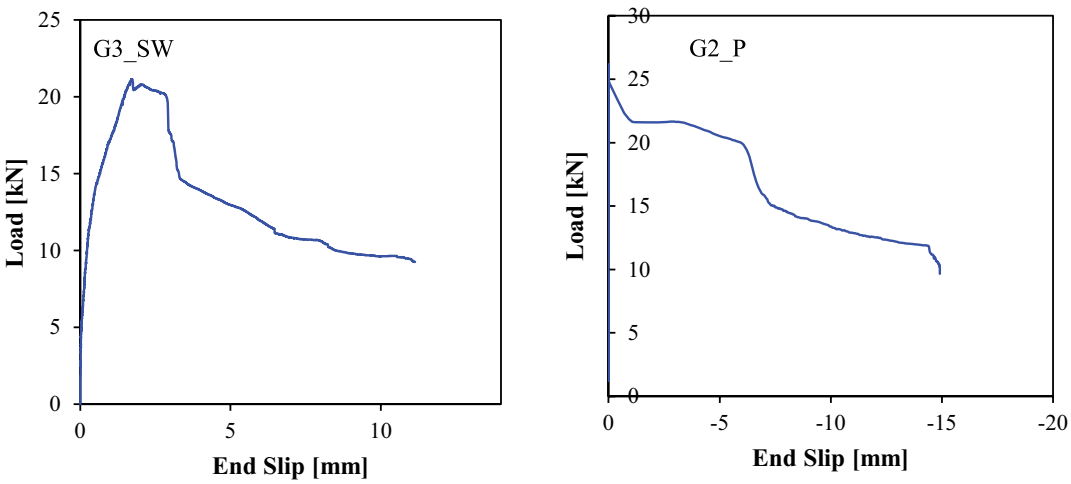

Fig. 13 End-slip curves for corroded, laterally strengthened beams.

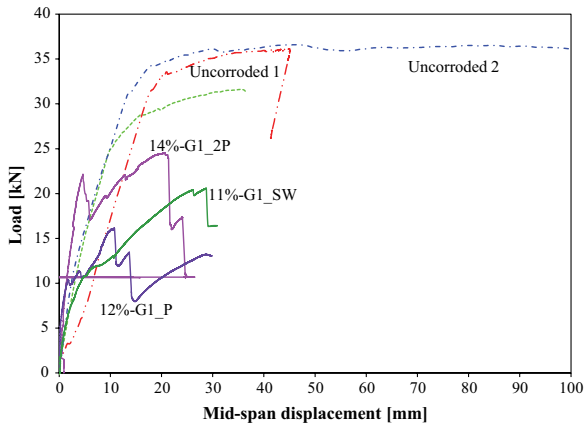

Fig. 14 Load vs. mid-span deflection curves for corroded unstrengthened beams and uncorroded beams.

bond-slip performance. Moreover, the decrease in bond capacity after peaking that was experimentally observed was less pronounced than exhibited by the curves presented within CEB-FIP Model Code 90.

4 Modelling the Structural Behaviour of RC Members

A 3D, non-linear, macro-scale, finite-element method (FEM) model of the statically indeterminate RC beams utilised within the experiment was developed to investigate the structural behaviour of the RC beams when varying levels of reinforcing steel corrosion was incurred. The aim of the FEM model was to assess the adequacy of different local bond-slip relationships and to reproduce the effects of corrosion on embedded steel reinforcement elements. The software program 'DIANA' in conjunction with the pre- and post-processor Midas FX+ (Diana et al. 2015) was utilised for the numerical simulations. The experimental results were then utilised to validate the findings of the FEM model.

4.1 FEM Model Development

Because of the symmetry of the experimental test setup, only half of the RC beam was modelled. The central support was represented as being perfectly fixed in all degrees of freedom. The outer support was represented as a pinned support. The existence of the neoprene bearing plates was simulated in the model for both the supports and the applied load point in order to avoid local, undesired crushing phenomena due to localised stress or geometrical configuration of the mesh. Beam loading was implemented by controlling the displacement of the applied load point. The beam self-weight was not included in the FEM model as it was considered negligible with respect to the total applied load.

Different element types were utilised within the developed model: 3D tetrahedral elements (type TE12L) for concrete; 1D truss-bar embedded elements (L2TRU) for reinforcement steel; and, interface elements (L8IF)

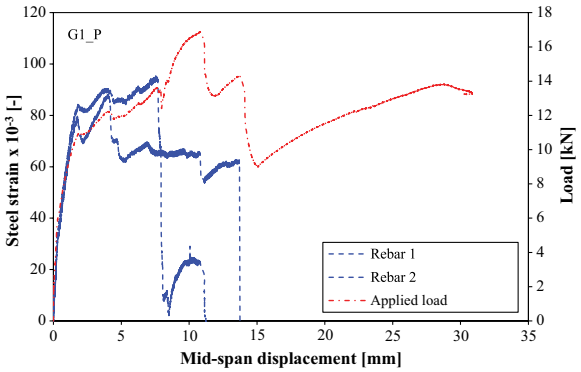

Fig. 16 Evolution of strain in bottom reinforcement up to failure.

Fig. 15 Final appearance of corroded beams, showing splitting and spalling.

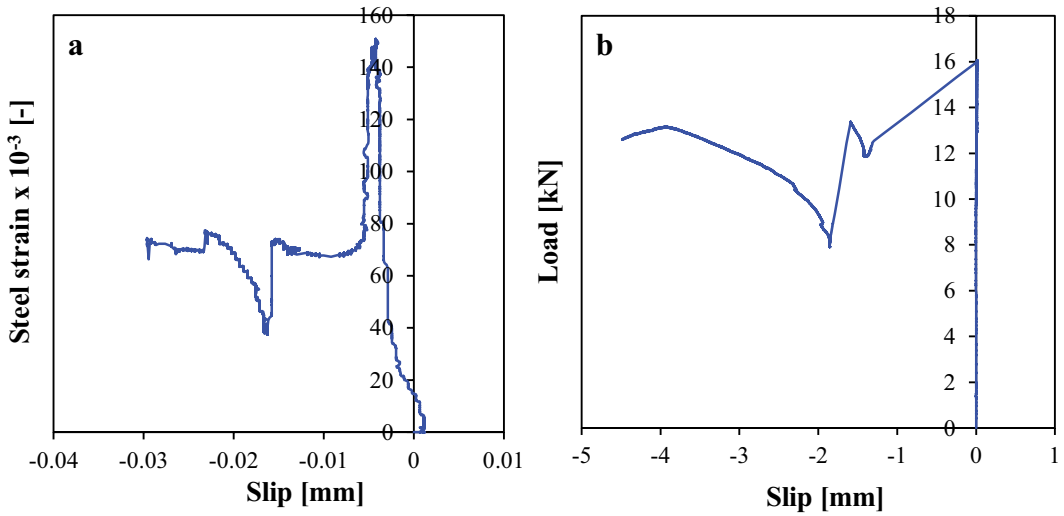

Fig. 17 **a** End slip vs. steel strain, **b** end slip vs. applied load, unstrengthened beam G1_P.

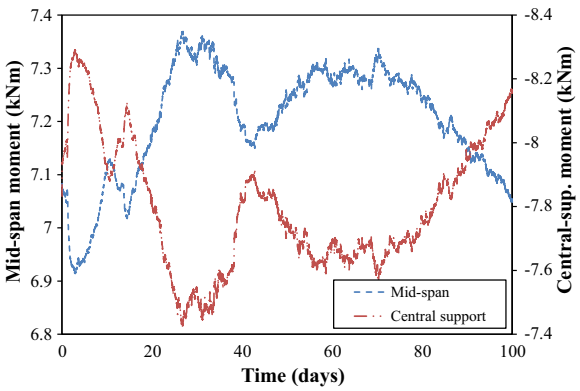

Fig. 18 Moment redistribution between mid-span and central support during the corrosion phase until collapse.

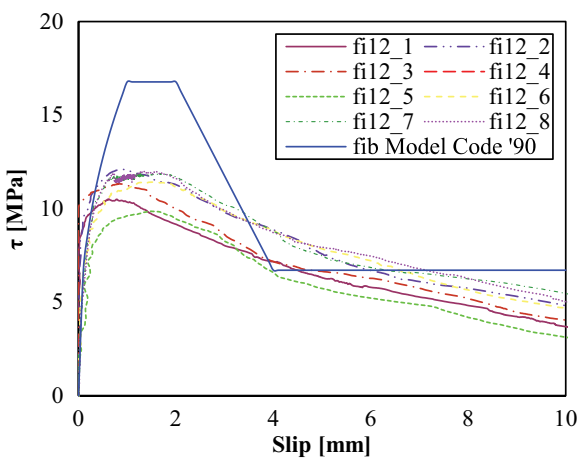

Fig. 19 Pull-out test results and fib Model Code [XX] bond-slip curve.

between the concrete and the reinforcement steel elements to consider the 1D bond-slip relationship. The use of embedded steel reinforcement allows defining the reinforcement wherever inside the concrete mother elements so that it is not necessary to re-mesh the concrete mesh including nodes along the reinforcement. The concrete elements were modified to reflect the incremental stiffness provided by the embedded steel reinforcement. Intersection nodes were internally created on the tetrahedral elements faces to define the interface elements between the concrete and the steel reinforcement. An overview of the developed FEM model is illustrated at Fig. 20.

4.2 Material Models

4.2.1 Concrete and Steel Reinforcement

Concrete behaviour was characterised by means of a constitutive model based on non-linear fracture mechanics using a total strain-based, smeared-crack model with rotating crack approach. The FEM model required the specification of the compressive behaviour and the tensile softening behaviour. A Thorenfeldt (Thorenfeldt et al. 1987) compression curve was utilised in order to more realistically describe the behaviour of the concrete in compression. The softening branch was adapted to the element size. The tensile behaviour of plain concrete was governed by a softening law as referenced (Cornelissen et al. 1986), using a fracture energy as calculated within CEB-FIP Model Code 90 (fib Model Code 1990). The concrete compressive strength that was utilised within the FEM model was identical to the concrete compressive strength obtained in the tests.

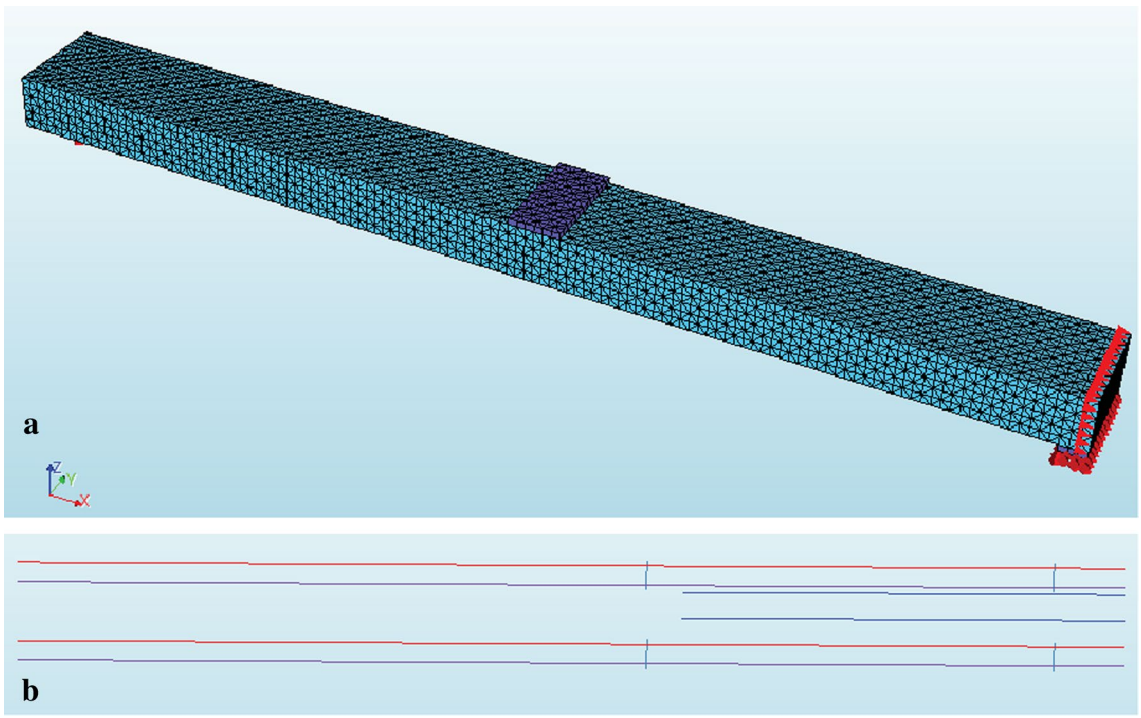

Fig. 20 **a** View of 3D mesh DIANA model. **b** Reinforcement elements.

The effects of corrosion on the mechanical properties of the steel reinforcement were taken into account within the FEM model. The model presented within reference (Fernandez et al. 2016a) was enhanced by incorporating corrosion of the steel (Bairan et al. 2011) and further validated within (Fernandez et al. 2016b; Diana et al. 2015), and it was used to define the mechanical properties of the corroded steel reinforcement. A reduction of the elastic limit and the steel strength is contingent upon the degree of corrosion. Figure 21 illustrates the different stress–strain curves utilised. A non-linear material model for steel was implemented in the model, with an isotropic plasticity and Von Mises yielding criterion. In addition, post-yielding hardening behaviour was included; this behaviour considers the incremental stress incurred after the constant stress zone due to steel hardening. The remaining cross-section and the remaining perimeter of the reinforcing steel associated with each level of corrosion was also defined within the model's steel properties in order to be able to apply the different bond-slip relationships described in the following section. The outlined parameters were necessary to describe the stress transfer to the concrete and to obtain the reinforcement slips.

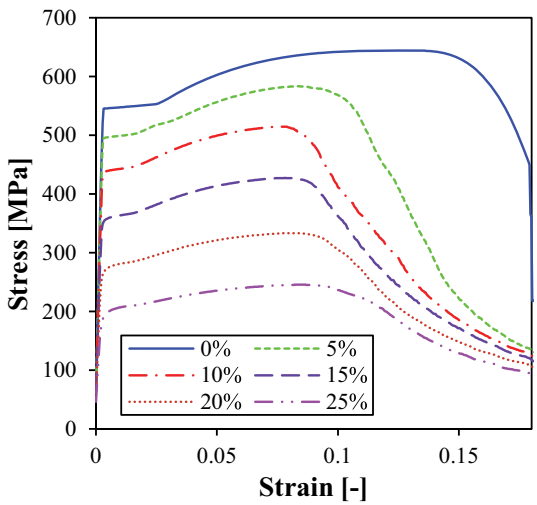

Fig. 21 Mechanical properties for corroded steel as input for numerical analysis (Fernandez et al. 2016a).

4.2.2 Bond-Slip Model

The bond between the concrete and steel reinforcement bars was modelled by means of the embedded reinforcing steel approach with non-linear bond-slip relationship, using interface elements as defined in the DIANA software documentation (Diana et al. 2015). User-supplied multi-linear curves could be utilised as model input values. The local bond-slip behaviour utilised within the FEM model was based on the approach

outlined by Lundgren et al. (2012). Input to the FEM model was based on the local bond-slip defined within CEB-FIP Model Code 90 (fib Model Code 1990) or by user-supplied, uncorroded bond-slip values. The specimen parameters, such as the amount of transversal reinforcement, concrete cover, diameter of the anchored reinforcement, concrete compressive strength and the measured degree of corrosion were taken into account. Corrosion of the steel reinforcement was accounted for by shifting the uncorroded bond-slip curve along the slip axis utilising a specific calibrated value (Fig. 22). Consideration for the variation of the confinement conditions due to splitting cracks was also considered within the FEM model.

For the internal RC beam strips, the local bond-slip curves for the uncorroded, steel reinforcement were extracted from the experimental test results and utilised as input to the analytical model.

For the external strips, the reduced concrete cover implied reduced confinement conditions; thus, the experimental bond-slip curves were considered unrealistic (from tests with concrete covers of 90 mm) and a bond-slip curve based on the local bond-slip curves presented within CEB-FIP Model Code 90 (fib Model Code 1990) were utilised for input values.

In both analytical cases (internal strip and external strip) the corroded bond-slip curves were calculated accordingly within Lundgren et al. (2012); the bond-slip curves utilised are detailed within Fig. 23.

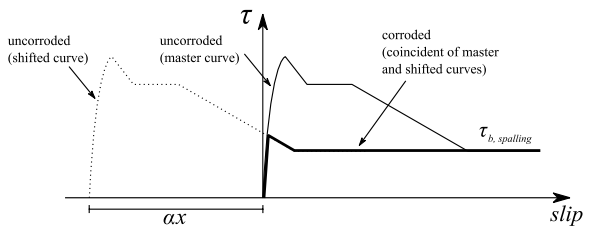

Fig. 22 Scheme of a local bond-slip curve for 'good' bond conditions; the curve is an interpolation of confined and unconfined cases.

4.3 Discussion of FEM Numerical Analyses

A comparison between the FEM model results and the experimental results for selected RC beams is presented within the following sections.

4.3.1 Uncorroded RC Beam Specimens

Figure 24 illustrates the parameters measured on the experimental uncorroded RC beam member as compared to the numerical results obtained from the FEM model. In general, there was a good agreement with regard to overall structural behaviour between the numerical analysis results and the experimental test results as demonstrated by the numerical analysis calculating similar ultimate loads as those encountered within the experiment (Fig. 24a). However, the FEM model did not fully accommodate the post yielding and pull-out behavioural parameters exhibited within the experiment; the lack of adjustment for these parameters resulted in convergence problems associated with large displacements. A potential reason to explain the lack of agreement within the FEM model could be attributed to inaccuracies in the definition of the bond-slip and fracture energy. The bond-slip data obtained from the experimental pull-out test represented very good confinement conditions as the concrete cover over/around the steel reinforcement bar was more than five times the bar's diameter (12 mm). The concrete cover of the steel reinforcement bar within

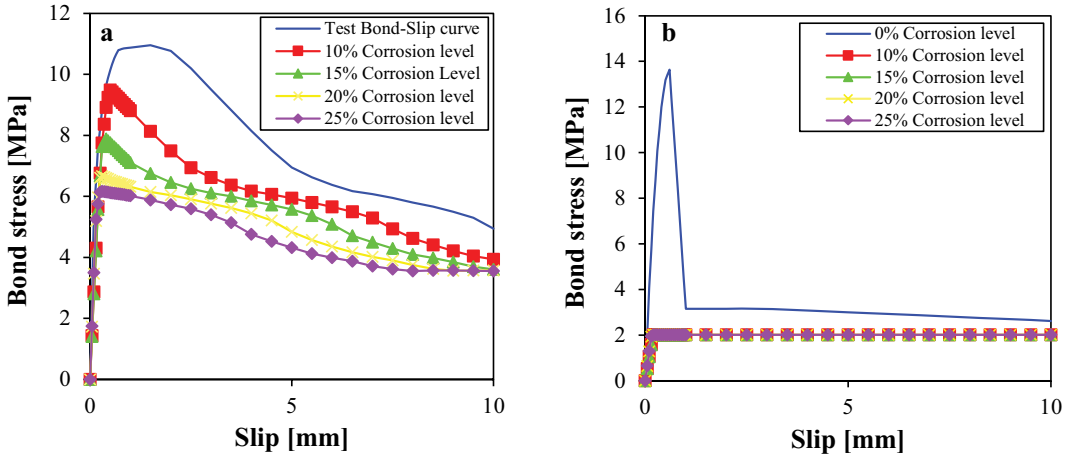

Fig. 23 **a** Confined conditions. **b** Unconfined conditions.

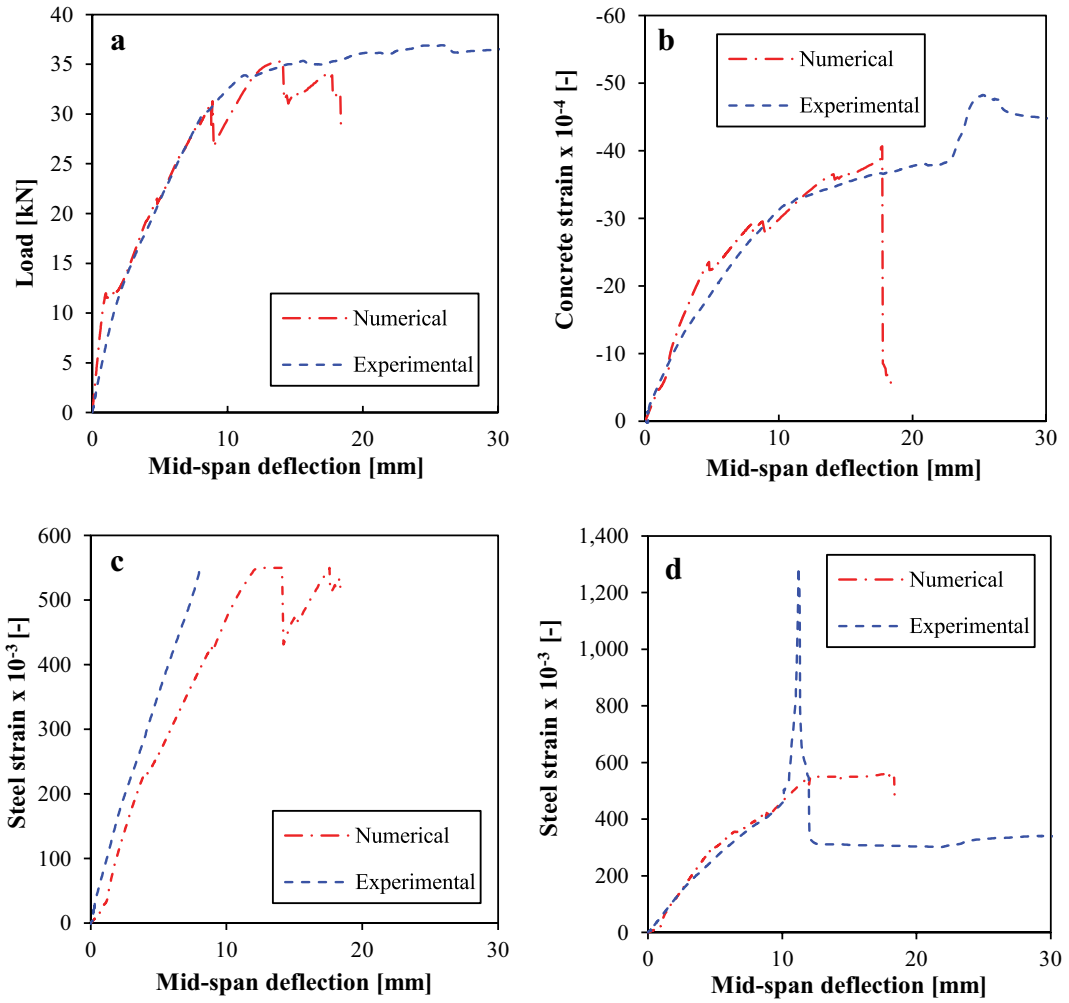

Fig. 24 Uncorroded beams: numerical analysis vs. experimental results. **a** Load vs. mid-deflection, **b** Mid-span top fiber concrete strain vs- mid-span deflection, **c** Top reinforcement strain at central support vs. mid-span deflection, **d** Bottom reinforcement strain at mid-span vs. mid-span deflection.

the RC beam member however was only 15 mm (slightly larger than one 12 mm reinforcement bar diameter) and despite the confinement provided by the external passive strengthening, the level of confinement associated with the RC beam was not the same as the level of confinement associated with the pull-out tests. Additionally, no experimental tests for the fracture energy were performed; the fracture energy parameter that was obtained for use within the FEM model was based on the expressions described within CEB-FIP Model Code 90 (fib Model Code 1990).

The stresses within the tensile steel reinforcement bars and the concrete stresses in the midspan zone of the RC beam members were representatively calculated by the FEM model as demonstrated by the agreement between the results of the numerical analysis and the measured experimental results (Fig. 24b–d).

4.3.2 Corroded RC Beam Specimens

A good agreement between the experimental results and the FEM model results for the internal RC beam strips was achieved. Figure 25 details the overall behaviour of four RC beams, comparing the experimental versus numerically-derived load–displacement curves. The maximum loading numerically derived agreed well with the maximum loading attained experimentally. The failure of the different RC beam specimens was also well reproduced by the FEM model despite the convergence problems discovered after the last crack occurrence. Figure 26 provides a comparison between the numerical and the measured strains on the bottom reinforcement for RC beam specimen G2_SW. The material model utilised for the corroded steel as employed within the FEM model indicated yielding of steel reinforcement for this strain level; the numerical

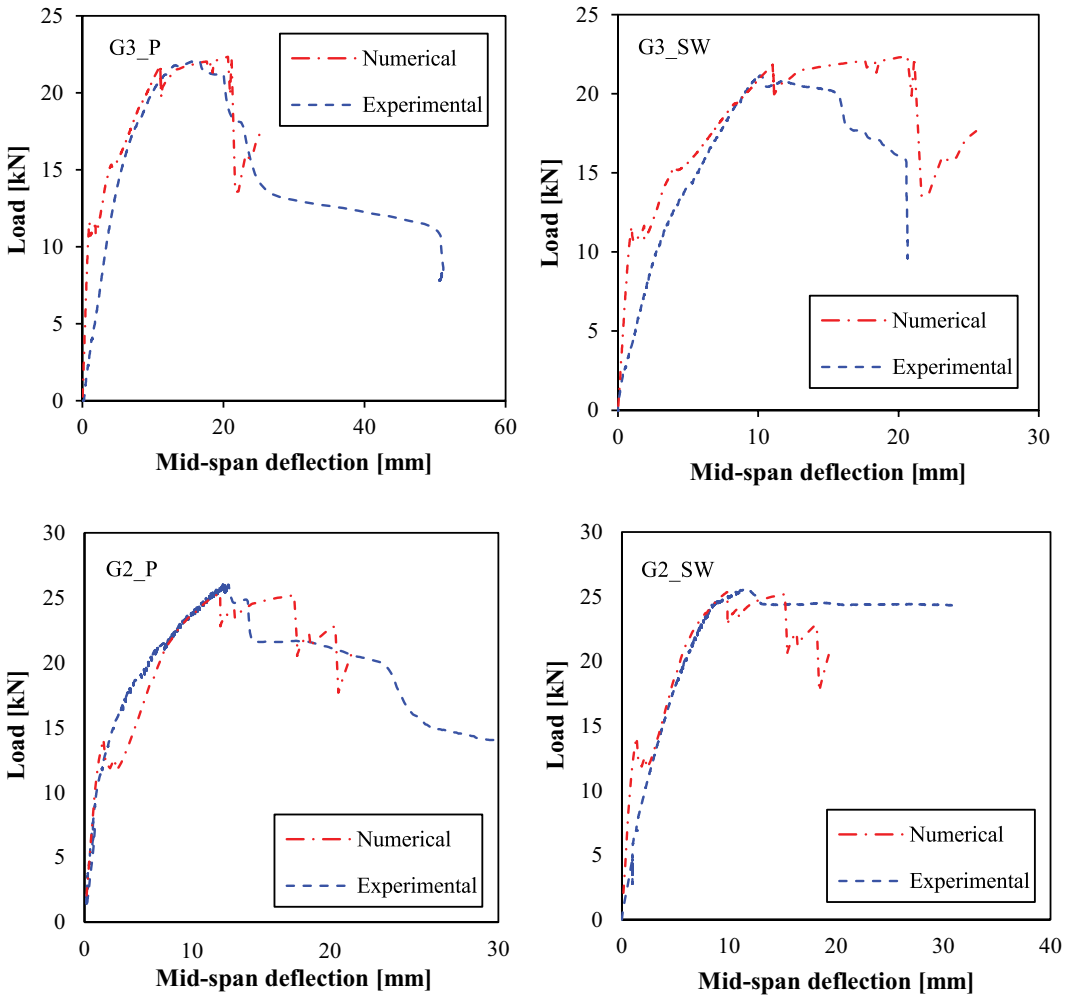

Fig. 25 Corroded, laterally strengthened beams: numerical analysis vs. experimental results. Load vs. mid-span deflections.

analysis values mimicked those measured within the experiment.

The results of the numerical model of the external strips (unstrengthened beams) did not correlate well to the experimental results. In general, the numerical models calculated up to 30% more capacity than their experimental counterparts; the discrepancy was attributed to the bond model used. The input data for the bond-slip relationship was an interpolation from the CEB-FIP Model Code 90. Moreover, the embedded bond model offered by DIANA is a uniaxial model; no splitting stresses normal to the longitudinal steel bar direction are directly accounted for. The splitting effects due to the normal stresses are indirectly included in the local bond-slip relationship by decreasing its capacity simulating splitting failure. Hence, the inclusion of such relationships may lead to overestimated anchorage lengths and residual bond capacity, resulting in an increased ultimate capacity. Therefore, the utilisation of simplified 1D bond-slip models may result in high inaccuracies when describing anchorage failure due to splitting and the push out of steel reinforcement. This 1D bond-slip model problem was also reported within reference (Tahershamsi et al. 2017). Consequently, the use of more advanced modelling approaches that account for splitting effects would be more suitable to reproduce the structural behaviour in such situations.

4.3.3 Modelling Approaches for the Assessment of Corroded RC Structures

Different approaches have been followed in the current state of the art for the modelling of the structural effects of corrosion of steel reinforcement in RC structures. As it is reflected in many studies and in the present work, the effects of corrosion on the structural behavior are very wide and complex (Fernandez et al. 2015; Tahershamsi

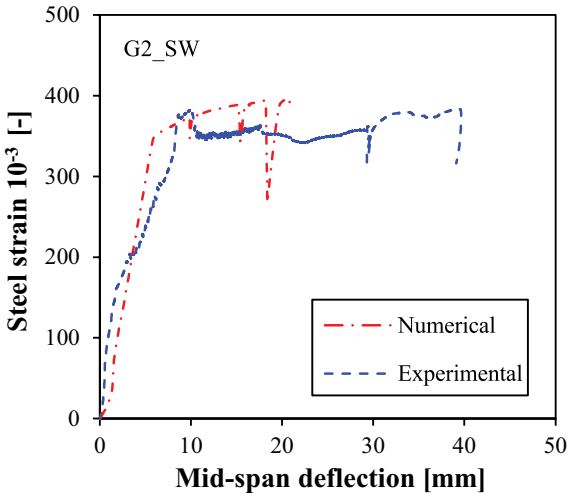

Fig. 26 Corroded, laterally strengthened beam: numerical analysis vs. experimental results. Mid-span deflection vs. bottom reinforcement.

et al. 2014; Berrocal et al. 2017; Malumbela et al. 2009b; Cairns et al. 2005; Cobo et al. 2011; Stewart 2009; Law et al. 2008; Zhu et al. 2013). One of the most relevant structural effects of corrosion of reinforcing steel bars are those derived from the change of the interaction between the concrete and steel, namely bond behavior. In order to adequately capture the effects of corrosion on bond ermine, adequate models, consistent with the level of idealization of the structures (1D or 3D) are required. For example, in order to capture local effects, full interaction models that account for the multiaxial stress state around the steel bar are necessary for a realistic representation of the corrosion effects on the structure. Such models require the development of 3D solid models that can cope with the full description of the bond interaction (Berrocal et al. 2017; Jansson et al. 2012; Lundgren 2002; Ožbolt et al. 2011).

Nevertheless, some efforts have been carried out to perform simplifications in the modelling approaches for two reasons. First, the need to reduce the computational cost and to extend the scope of the modelling to a larger part of the structure; second, to provide simplified models and tools which can implemented in ordinary engineering practice assessments in a cost/time efficient way. To pursue such simplifications, the integration of some of the aforementioned multi-directional effects has been carried out into simpler models such as 3D beam elements or analytical expressions that can account for some of the described effects (Biondini and Vergani 2014; Fernandez et al. 2016c; Stewart 2009; Biondini et al. 2004; Ferreira et al. 2014; Bernat et al. 2012; Oliveira 2008). In addition, new approaches to reproduce the 3D complex behavior of the bond effects in RC concrete beams have been developed to include some of the multiaxial effects in simple bond slip relations that have proven to be on the safe side for the analysis of complex problems such as anchorage capacity of corroded bars (Tahershamsi et al. 2017; Lundgren et al. 2012; Blomfors et al. 2018; Zhang et al. 2009; Bhargava et al. 2007).

However, according to the experimental observations presented by some authors (Fernandez et al. 2016c; Zhang et al. 2009; Malumbela et al. 2009a) and the results in Sect. 4 and in (Rodriguez et al. 1997; Lundgren et al. 2015), it should be noted that the demand of performance of the numerical models of RC structures is different for adequately capturing the structural response at Serviceability or at Ultimate load levels. For service load levels, simplified bond-slip relations between concrete and steel have proven to be reliable to describe the structural behavior in a reasonable manner. To describe complex ultimate states of the structure, a higher level of modelling might be required, which should be able to capture in a trustworthy manner phenomena such as change in the failure mode (i.e. anchorage failure or bending to shear failure), loss of bond or splitting stresses (including confinement loss effects) among others.

5 Conclusions

Conclusions of the study on the ultimate capacity of corroded statically indeterminate reinforced concrete members are as follows:

1. Premature, brittle anchorage failure due to splitting of RC beam specimens simulating external unconfined strips of a plate (laterally unstrengthened) resulted in a reduction in the loading capacity by up to 55%. Internal strips (laterally strengthened, simulating confined conditions) demonstrated a higher bearing capacity than the external strips even when higher corrosion levels were present. Reduction in the loading capacity between 26 and 39% were observed within corrosion levels varying from between 15 and 24% were observed.
2. Despite higher levels of corrosion exposure, internal strip members (where no premature loss of anchorage capacity takes place) exhibited up to a 30% higher redistribution of internal moments over those observed within uncorroded beam specimens. A higher redistribution of internal moments is realised as the loss of steel reinforcement in highly damaged cross-sections produces imposed deformations and displacements; the imposed deformations and displacements subsequently generate secondary (compatibility) moments within a statically indeterminate structure. These secondary moments reduce

moment demand within the highly damaged zone while increasing the moment within the less damaged regions of the RC beam.

3. As a consequence of conclusions 1 and 2, we contend that structural redundancy generates a beneficial indirect structural effect (reduction of the demand in deteriorated cross-sections) as opposed to the harmful structural effect directly produced by corrosion (reduction of cross-section capacity) thereby mitigating the reduction in carrying capacity and affording higher safety levels compared to simply supported members. The impact of pitting or very localised corrosion has proven to be very harmful to structural capacity with a potential reduction of up to 56% in the ultimate capacity of a RC beam.
4. The bond between the concrete and the reinforcing steel is a key parameter that affects structural response. In all cases, very high corrosion levels produced a severe deficiency in the bond; the bond deficiency in turn primarily controls the failure mode and load bearing capacity of the specimens. Other local effects, such as degradation of the corroded steel mechanical properties, are more significant at low corrosion levels or on more confined specimens. However, the numerical analysis that was conducted demonstrates that the inclusion of such effects is relevant to adequately reproduce structural performance in ultimate state conditions.
5. 3D FEM models that utilise 1D bond-slip relationships and incorporate the corrosion phenomena detailed within this study are suitable to reproduce the structural behaviour of a corroded structure. Nevertheless, these kinds of 3D FEM models cannot reproduce brittle anchorage failure due to splitting as result of conditions where confinement has been severely compromised (primarily when the push-out effect of steel reinforcement is developed).
6. More complex bond models that can model the full interaction, i.e. that account not only for simple shear stresses but coupled longitudinal/normal stresses to the steel bar, are required to better predict/reproduce actual structural behaviour when the risk of steel reinforcement push-out exists. Modelling needs to account for splitting stresses and no-bond capacity of the steel reinforcement.

Authors' contributions

IF planned and carried out the experimental and numerical studies of the beams and drafted the manuscript. MFH and ARM contributed in the planification and designing of the experimental and numerical studies and the writing of the manuscript by providing discussion and cooperation and commenting the text. JMB contributed providing discussion and cooperation. All authors read and approved the final manuscript.

Author details

[1] Department of Architecture and Civil Engineering, Division of Structural Engineering, Concrete Structures, Chalmers University of Technology, 412 96 Gothenburg, Sweden. [2] Department of Construction Technology, Universidade da Coruña, Campus de Elviña, 15172 A Coruña, Spain. [3] Department of Civil and Environmental Engineering, Division of Structures, Materials and Construction Engineering, Polytechnic University of Catalonia, Barcelona, Spain.

Acknowledgements

The authors wish to acknowledge the financial support of the European Regional Development Fund (ERDF) and The Ministry of Economy and Competitiveness of the Government of Spain (MINECO) for providing funds for projects BIA2009-11764, BIA2015-64672-C4-1-R, BIA2015-64672-C4-2-R. The financial support of Infrastructures de Catalunya (ICAT) was also highly appreciated.

Competing interests

The authors declare that they have no competing interests.

Availability of data and materials

Not applicable.

Consent for publication

Not applicable.

Ethics approval and consent to participate

Not applicable.

Funding

Not applicable.

Publisher's Note

Received: 19 March 2018 Accepted: 4 July 2018
Published online: 28 November 2018

References

Apostolopoulos, C. A., Diamantogiannis, G., & Apostolopoulos, A. C. (2016). Assessment of the mechanical behavior in dual-phase steel B 400 C, B 450 C, and B 500 B in a marine environment. *Journal of Materials in Civil Engineering, 28,* 1–9. https://doi.org/10.1061/(ASCE)MT.1943-5533.0001271.

Austin, S. A., Lyons, R., & Ing, M. J. (2004). Electrochemical behavior of steel-reinforced concrete during accelerated corrosion testing. *Corrosion, 60,* 203–212. https://doi.org/10.5006/1.3287722.

Bairan, J. M., Marí, A. R., Ortega, H., & Rosa, J. C. (2011). Effects of winding and straightening of medium and large diameter reinforcing bars manufactured in coils in their mechanical properties. *Materiales de Construcción, 61,* 559–581. https://doi.org/10.3989/mc.2011.60110.

Ballim, Y., & Reid, J. C. C. (2003). Reinforcement corrosion and the deflection of RC beams—an experimental critique of current test methods. *Cement and Concrete Composites, 25,* 625–632. https://doi.org/10.1016/S0958-9465(02)00076-8.

Bernat, A. M., García, J. M. B., Ibars, E. O., & Perez, I. F. (2012). Numerical simulation of the structural effects of the deterioration in concrete structures. In: *Proceedings of fib Symposium "Concrete Structures for Sustainable Community".*

Berrocal, C. G., Fernandez, I., Lundgren, K., & Löfgren, I. (2017). Corrosion-induced cracking and bond behaviour of corroded reinforcement bars in SFRC. *Composites Part B: Engineering*. https://doi.org/10.1016/j.compositesb.2017.01.020.

Bhargava, K., Ghosh, A. K., Mori, Y., & Ramanujam, S. (2007). Corrosion-induced bond strength degradation in reinforced concrete-Analytical and empirical models. *Nuclear Engineering and Design, 237,* 1140–1157. https://doi.org/10.1016/j.nucengdes.2007.01.010.

Biondini, F., Bontempi, F., Frangopol, D. M., & Malerba, P. G. (2004). Cellular automata approach to durability analysis of concrete structures in aggressive environments. *Journal of the Structural Engineering, 130,* 1724–1737. https://doi.org/10.1061/(ASCE)0733-9445(2004)130:11(1724).

Biondini, F., & Vergani, M. (2014). Deteriorating beam finite element for nonlinear analysis of concrete structures under corrosion. *Structure and Infrastructure Engineering, 11,* 519–532. https://doi.org/10.1080/15732479.2014.951863.

Blomfors, M., Zandi, K., Lundgren, K., & Coronelli, D. (2018). Engineering bond model for corroded reinforcement. *Engineering Structures, 156,* 394–410. https://doi.org/10.1016/J.ENGSTRUCT.2017.11.030.

Broomfield, J. (2002). *Corrosion of steel in concrete: understanding, investigation and repair* (2nd ed.). Abingdon: Taylor & Francis.

Cabrera, J. G. (1996). Deterioration of concrete due to reinforcement steel corrosion. *Cement and Concrete Composites, 18,* 47–59.

Cairns, J., & Millard, S. (1999). Reinforcement corrosion and its effect on residual strength of concrete structures. In *Proceeding 8th international conference on structure*. Faults Repair, Edinburg, UK.

Cairns, J., Plizzari, G. A., Du, Y., Law, D. W., & Franzoni, C. (2005). Mechanical properties of corrosion-damaged reinforcement. *ACI Materials Journal*, *102*(4), 256–264. https://doi.org/10.14359/14619.

Caré, S., Nguyen, Q. T., L'Hostis, V., & Berthaud, Y. (2008). Mechanical properties of the rust layer induced by impressed current method in reinforced mortar. *Cement and Concrete Research, 38,* 1079–1091. https://doi.org/10.1016/j.cemconres.2008.03.016.

Cobo, A., Moreno, E., & Cánovas, M. F. (2011). Variación de las características mecánicas de armaduras de alta ductilidad B500SD en función de su grado de corrosión. *Materiales de Construcción, 61,* 517–532. https://doi.org/10.3989/mc.2011.61410.

Cornelissen, H. A. W., Hordijk, D. A., & Reinhardt, H. W. (1986). Experimental determination of crack softening characteristics of normalweight and lightweight concrete. *Heron, 31,* 45–56.

Coronelli, D. (2002). Corrosion cracking and bond strength modeling for corroded bars in reinforced concrete. *ACI Structural Journal*, *99*, 267–276. http://www.scopus.com/inward/record.url?eid=2-s2.0-0036590277&partnerID=40&md5=b6dd246bbc59b433496286431d46a021.

Dang, V. H., & François, R. (2013). Influence of long-term corrosion in chloride environment on mechanical behaviour of RC beam. *Engineering Structures, 48,* 558–568. https://doi.org/10.1016/j.engstruct.2012.09.021.

Diana, TNO Diana. (2015). Finite element analysis user's manual—release 9.6.6. Delft: TNO.

Fernandez, I., Bairán, J. M., & Marí, A. R. (2015). Corrosion effects on the mechanical properties of reinforcing steel bars. Fatigue and σ–ε behavior. *Construction and Building Materials, 101,* 772–783. https://doi.org/10.1016/j.conbuildmat.2015.10.139.

Fernandez, I., Bairán, J. M., & Marí, A. R. (2016a). Mechanical model to evaluate steel reinforcement corrosion effects on σ–ε and fatigue curves. Experimental calibration and validation. *Engineering Structures*. https://doi.org/10.1016/j.engstruct.2016.03.055.

Fernandez, I., Bairán, J. M., & Marí, A. R. (2016b). 3D FEM model development from 3D optical measurement technique applied to corroded steel bars. *Construction and Building Materials, 124,* 519–532. https://doi.org/10.1016/j.conbuildmat.2016.07.133.

Fernandez, I., Herrador, M. F., Marí, A. R., & Bairán, J. M. (2016c). Structural effects of steel reinforcement corrosion on statically indeterminate reinforced concrete members. *Materials and Structures, 49,* 4959–4973. https://doi.org/10.1617/s11527-016-0836-2.

Fernandez, I., Lundgren, K., & Zandi, K. (2018). Evaluation of corrosion level of naturally corroded bars using different cleaning methods, computed tomography, and 3D optical scanning. *Materials and Structures*. https://doi.org/10.1617/s11527-018-1206-z.

Ferreira, D., Bairán, J., & Marí, A. (2014). Efficient 1D model for blind assessment of existing bridges: simulation of a full-scale loading test and comparison with higher order continuum models. *Structure and Infrastructure Engineering*. https://doi.org/10.1080/15732479.2014.964734.

fib model code. (1990). *CEB-FIP model code 1990 design code*. Lausanne.

Jansson, A., Lofgren, I., Lundgren, K., & Gylltoft, K. (2012). Bond of reinforcement in self-compacting steel-fibre-reinforced concrete. *Magazine of Concrete Research, 64,* 617–630. https://doi.org/10.1680/macr.11.00091.

Law, D., Du, Y., & Cairns, J. (2008). Structural performance of corrosion-damaged concrete beams. *Magazine of Concrete Research, 60,* 359–370. https://doi.org/10.1680/macr.2007.00102.

Losberg, A. (1962). *Cracks in continuous concrete road slabs and other concrete structures locked against movements from temperature and shrinkage* (Vol. 607, p. 45). Göteborg: Chalmers University of Technology.

Lu, C., Jin, W., & Liu, R. (2011). Reinforcement corrosion-induced cover cracking and its time prediction for reinforced concrete structures. *Corrosion Science, 53,* 1337–1347. https://doi.org/10.1016/j.corsci.2010.12.026.

Lundgren, K. (2002). Modelling the effect of corrosion on bond in reinforced concrete. *Magazine of Concrete Research, 54,* 165–173. https://doi.org/10.1680/macr.2002.54.3.165.

Lundgren, K., Kettil, P., Hanjari, K. Z., Schlune, H., & Roman, A. S. S. (2012). Analytical model for the bond-slip behaviour of corroded ribbed reinforcement. *Structure and Infrastructure Engineering, 8,* 157–169. https://doi.org/10.1080/15732470903446993.

Lundgren, K., Tahershamsi, M., Zandi, K., & Plos, M. (2015). Tests on anchorage of naturally corroded reinforcement in concrete. *Materials and Structures, 48,* 2009–2022. https://doi.org/10.1617/s11527-014-0290-y.

Malumbela, G., Alexander, M., & Moyo, P. (2009a). Steel corrosion on RC structures under sustained service loads—A critical review. *Engineering Structures, 31,* 2518–2525. https://doi.org/10.1016/j.engstruct.2009.07.016.

Malumbela, G., Moyo, P., & Alexander, M. (2009b). Structural behaviour of beams under simultaneous load and steel corrosion. In *Proceedings of ICCRRR* (pp. 646–650). Cape Town, South Africa.

Malumbela, G., Moyo, P., & Alexander, M. (2009b). Behaviour of RC beams corroded under sustained service loads. *Construction and Building Materials, 23,* 3346–3351. https://doi.org/10.1016/j.conbuildmat.2009.06.005.

Oliveira, R. S., Ramalho, M. A., & Corrêa, M. R. S. (2008). A layered finite element for reinforced concrete beams with bond-slip effects. *Cement and Concrete Composites, 30,* 245–252. https://doi.org/10.1016/j.cemconcomp.2007.09.007.

Ožbolt, J., Balabanić, G., & Kušter, M. (2011). 3D Numerical modelling of steel corrosion in concrete structures. *Corrosion Science, 53,* 4166–4177. https://doi.org/10.1016/J.CORSCI.2011.08.026.

Rodriguez, J., Ortega, L., & Casal, J. (1997). Load carrying capacity of concrete structures with corroded reinforcement. *Construction and Building Materials, 11,* 239–248. https://doi.org/10.1016/S0950-0618(97)00043-3.

Ruiz, M. F., Muttoni, A., & Gambarova, P. G. (2007). Analytical modeling of the pre-and postyield behavior of bond in reinforced concrete. *Journal of Structural Engineering, 133,* 1364–1372.

El Maaddawy, T. E. A., & Soudki, K. K. A. (2003). Effectiveness of impressed current technique to simulate corrosion of steel reinforcement in concrete. *Journal of Materials in Civil Engineering*. 41–47. Retrieved July 3, 2014, from http://ascelibrary.org/doi/abs/10.1061/(ASCE)0899-1561(2003)15:1(41).

Stewart, M. G. (2009). Mechanical behaviour of pitting corrosion of flexural and shear reinforcement and its effect on structural reliability of corroding RC beams. *Structural Safety, 31,* 19–30. https://doi.org/10.1016/j.strusafe.2007.12.001.

Tahershamsi, M., Fernandez, I., Lundgren, K., & Zandi, K. (2016). Hanjari, investigating correlations between crack width, corrosion level and anchorage capacity. *Structure and Infrastructure Engineering, 2479,* 1–14. https://doi.org/10.1080/15732479.2016.1263673.

Tahershamsi, M., Fernandez, I., Zandi, K., & Lundgren, K. (2017). Four levels to assess anchorage capacity of corroded reinforcement in concrete. *Engineering Structures*. https://doi.org/10.1016/j.engstruct.2017.06.024.

Tahershamsi, M., Zandi, K., Lundgren, K., & Plos, M. (2014). Anchorage of naturally corroded bars in reinforced concrete structures. *Magazine of Concrete Research, 66,* 729–744. https://doi.org/10.1680/macr.13.00276.

Thorenfeldt, E., Tomaszewicz, A., & Jensen, J. J. (1987). Mechanical properties of high-strength concrete and applications in design. In: *Concference utilization of high strength concrete*. Norway: Stavanger.

Torres-Acosta, A. A., Navarro-Gutierrez, S., & Terán-Guillén, J. (2007). Residual flexure capacity of corroded reinforced concrete beams. *Engineering Structures, 29,* 1145–1152. https://doi.org/10.1016/j.engstruct.2006.07.018.

UNE-EN_10080 = 2006, 2006.

Val, D. V., Stewart, M. G., & Melchers, R. E. (1998). Effect of reinforcement corrosion on reliability of highway bridges. *Engineering Structures, 20,* 1010–1019. https://doi.org/10.1016/S0141-0296(97)00197-1.

Zhang, R., Castel, A., & François, R. (2009). Serviceability limit state criteria based on steel–concrete bond loss for corroded reinforced concrete in

chloride environment. *Materials and Structures, 42,* 1407–1421. https://doi.org/10.1617/s11527-008-9460-0.

Zhu, W., François, R., Coronelli, D., & Cleland, D. (2013). Effect of corrosion of reinforcement on the mechanical behaviour of highly corroded RC beams. *Engineering Structures, 56,* 544–554. https://doi.org/10.1016/j.engstruct.2013.04.017.